The Event-specific Geomorphological Instantaneous Unit Hydrograph (E-GIUH): The basin hydrological response characteristic of a flood event

Hervé Andrieu, Roger Moussa, Pierre-Emmanuel Kirstetter

The Event-specific Geomorphological Instantaneous Unit Hydrograph (E-GIUH): The basin hydrological response characteristic of a flood event

Hervé Andrieu[1], Roger Moussa[2], Pierre-Emmanuel Kirstetter[3,4,5,6]

[1] GERS-LEE, Univ. Gustave Eiffel, IFSTTAR, F-44344 Bouguenais, France

[2] LISAH, Univ. Montpellier, INRAE, IRD, Montpellier SupAgro, Montpellier, France

[3] School of Civil Engineering and Environmental Science, University of Oklahoma, Norman, OK 73072, USA
[4] School of Meteorology, University of Oklahoma, Norman, OK 73072, USA
[5] Advanced Radar Research Center, University of Oklahoma, Norman OK 73072, USA
[6] NOAA / National Severe Storms Laboratory, Norman OK 73072, USA

Submitted for publication in the Journal of Hydrology
https://doi.org/10.1016/j.jhydrol.2021.127158

Corresponding author: Hervé Andrieu, AndrieuHerve@orange.fr

Keywords : GIUH, Flash-flood, rainfall-runoff modeling, Inverse method, Rainfall spatial variability

Highlights:

- The Width Function-GIUH has been modified to project the spatial distribution of rainfall onto the hydrological network.
- By accounting for the influence of rainfall on the hydrological response of catchments, an Event specific - GIUH (E-GIUH) is defined for each flood event.
- The identification of an E-GIUH from observed data (hydrograph and rain field time series) is treated as an inverse problem.
- The proposed identification method is applied to a sample of flooding events on two catchments within the OHMCV Observatory territory, in confirming the wide diversity of E-GIUHs.
- A sensitivity analysis indicates that the method is fairly robust and easy to use, which is most encouraging for large-scale applications.

Abstract:

In the field of hydrology, the Geomorphological Instantaneous Unit Hydrograph (GIUH) is central to describing a watershed response. The application of GIUH is extended to individual hydrological events by accounting for the influence of rainfall spatial distribution. A method is proposed herein to identify the Geomorphological Instantaneous Unit Hydrograph specific to each flood event (i.e. E-GIUH), when runoff of effective rainfall is the dominant process. The E-GIUH is derived from observational data, namely: rainfall field time series, and a hydrograph. Such an identification process is formulated as an inverse problem with parameters such as the E-GIUH velocity and coefficient of dispersion, as well as the hyetograph of rainfall excess. The proposed method is applied to several flood events across two mountainous catchments within the Cevennes-Vivarais Mediterranean Hydrometeorological Observatory territory prone to flash flooding. Results indicate that the E-GIUHs display significant variability over the two basins, and the E-GIUH parameters appear to be correlated with the flood event magnitude. The E-GIUH synthetizes the basin response to rain forcing and can be considered as a signature of flood events. A sensitivity study suggests that E-GIUH identification is fairly robust, even with respect to the *a priori* hyetograph of effective rainfall.

1. Introduction

The concept of the Geomorphological Instantaneous Unit Hydrograph (GIUH), defined as the probability density function (pdf) of water travel time along the channel links of the hydrographic network, was developed by (Gupta et al., 1980; Rodriguez-Iturbe and Valdés, 1979) by linking the unit hydrograph (Dooge, 1959; Sherman, L.K., 1932) to the geomorphological parameters of a catchment. The emergence of GIUH has contributed to the success of lumped rainfall-runoff models, which are widely used for their parsimony and robustness in both flash flood prediction and hydrograph analysis when runoff of effective rainfall is the dominant process of floods (Wood et al., 1990) . More specifically, the GIUH is well suited to treating the ungauged basin modeling problem, which pertains to the longstanding challenge of regional modeling over large areas, as exposed in the review paper by (Singh et al., 2014). The widespread use of GIUH within the hydrology community coupled with its development over the decades attests to its relevance in representing watershed responses and moreover confirms the ability of this approach to complement distributed models (Fatichi et al., 2016).

The initial GIUH formulation relies on the channel links in hydrographic networks, as described by the Horton classification. (Marani et al., 1991) and (Rodriguez-Iturbe and Rinaldo, 1997) extended this formulation to the probability density function (pdf) of hydrological distances to the basin outlet, as described by the Width Function (Kirkby, 1976), and went on to propose the Width Function Geomorphological Approach (D'Odorico and Rigon, 2003; Rigon et al., 2016). An assumption of constant velocity is adopted to convert the distribution of flow distances into a pdf of travel times along flow paths. The travel time pdf may be represented by the Advection Dispersion Equation (ADE) (Rinaldo et al., 1991) and a unique solution of the Diffusive Wave Equation (Hayami, 1951; Moussa, 1997). The GIUH is thus defined by the Width Function and the two parameters characterizing the ADE and DWE, i.e. flow velocity and coefficient of dispersion. (Saco and Kumar, 2002a) justified this constant velocity assumption by showing that varying flow path velocities can be taken into account by means of a kinematic-geomorphic dispersion that increases the coefficient of dispersion parameter.

GIUH applications often rely on a unique set of parameters in order to calibrate the model (e.g. (Boudhraâ et al., 2018; Chen et al., 2019; Choi et al., 2011; Moussa, 1997; Yao et al., 2014), thereby suggesting that a single representative GIUH can be associated with a catchment. However, several studies have highlighted the influence on the catchment response of: i) the rain spatial distribution (Emmanuel et al., 2017; Goni et al., 2019; Olivera and Maidment, 1999; Zoccatelli et al., 2010), and ii) the rain event magnitude (Rodriguez et al., 2005; Saco and Kumar,

2002b). These findings have been confirmed by the post-event analysis of floods, (Smith et al., 2005, 2002) among others, and simulation studies (Emmanuel et al., 2015; Volpi et al., 2012), hence acknowledging the GIUH limitations listed by (Rigon et al., 2016), who specifically noted these shortcomings when accounting for the rainfall distribution. Broadly speaking, these results indicate that the GIUH depends on rainfall-runoff processes that drive the flow dynamics in the hydrograph network. Consequently, every flood event can be characterized by its own GIUH, hereafter denoted as the E-GIUH, which is capable of enriching the signatures of hydrological processes driving the basin response to rainfall forcing at the flood event scale (McMillan, 2020).

This manuscript aims to advance the width function-based GIUH by: i) adapting its formulation in order to account for the influence of spatial rainfall variability, and ii) proposing a method to determine the E-GIUH for each flood event. First, the GIUH formulation is adapted to take into account the spatial rainfall pattern by means of replacing the width function by the rainfall width function (Emmanuel et al., 2015; Woods and Sivapalan, 1999). This improvement serves to overcome a key limitation of the GIUH, as highlighted by (Rigon et al., 2016). Second, a novel E-GIUH identification method based on observed data is developed and tested. The typical approach consists of assuming a production function and jointly calibrating the GIUH and the production function parameters; hence, results depend on the *a priori* production function. To address this problem, the original method proposed herein formulates Event-GIUH identification as an inverse problem (Menke, 2012; Tarentola, A., 2005). Inverse theory was defined by (Menke, 2012) as “a set of mathematical techniques for reducing data to obtain knowledge about the physical world on the basis of inferences drawn from observations”. Inverse techniques have been used in hydrology, e.g. by (Pan and Wood, 2013) to derive spatially distributed runoff, by (Fisher et al., 2020) for the purpose of determining spatially distributed continuous river discharge from discrete flow data, as well as by (Boudhraâ et al., 2018) to derive the hyetograph of effective rainfall from flow data. The E-GIUH is identified from the observed hydrograh and from an estimation of the hyetograph of effective rainfall. It is likely that this hyetograph influences the resulting E-GIUH. The use of an inverse algorithm makes it possible to explicitly consider the specific role of this hyetograph. It can be done by considering it as a set of parameters of the problem to solve. The algorithm is initialized by the priori information about this hyetograph which combines the estimation of the a-posteriori hyetograph and its accuracy. The inverse algorithm will give more or less importance to the a priori hyetograph according to its accuracy, and will propose an improved shape. More generally, the adopted framework is well adapted to considering the weight of data, a priori parameter values and model on the solution based on their accuracy. The proposed approach extends the domain of application of the

GIUH. It allows to characterize each event in terms of a specific E-GIUH that can be viewed as the signature of this event".

Section 2 presents an adaptation of the width function-based GIUH, which takes into account the spatial rainfall variability and develops the approach employed to identify the E-GIUH from observed data, namely the hydrograph and rainfall field time series. The case study serving to test the proposed E-GIUH identification method is described in Section 3. This case study combines a set of events affecting two basins located in Southern France. Section 4 provides the application conditions of this E-GIUH identification approach, and Second 5 discusses the results obtained. Section 6 concludes the manuscript.

2. Methods

2.1 The Event-specific Geomorphological Instantaneous Unit Hydrograph (E-GIUH)

This section introduces the spatial variability of rainfall in the derivation of the Width Function-based E-GIUH (D'Odorico and Rigon, 2003; Rigon et al., 2016). The travel time of water drops and the GIUH both depend primarily on the hydrological distance *L*, defined as the distance to the outlet from any point on the hydrological network. Let *w* be the width function of the basin, defined as the portion of the basin area at the hydrological distance L, which in addition represents the transverse extent of the basin at *L* (Rodriguez-Iturbe and Rinaldo, 1997). The spatial rainfall variability is represented by the rainfall variability along hydrological paths (Smith et al., 2005). The flow at the catchment outlet can be expressed as:

$$Q(t) = \int_0^{L_{max}} dQ(L,t)\, dL \quad with \;\; dQ(L,t) = A\, w(L)\, dL \int_0^t R_e(L, t-\tau)\, f(L,\tau)\, d\tau \tag{1}$$

with: $dQ(L,t)$ denoting the outflow at time *t* from surface area $dA = A\, w(L) dL$ at hydrological distance L; R_e the effective rainfall at time τ and at hydrological distance L; L_{max} the maximum hydrological distance; and f the travel time distribution of water particles from dA.

It is assumed that the probability density function (pdf) of travel time can be modeled by the following law (Rigon et al., 2016; Rinaldo et al., 1991):

$$f(L,t) = \frac{L}{\sqrt{4\pi D(L)\, t^3}}\; exp\left[-\frac{(L-U(L)t)^2}{4D(L)t}\right] \tag{2}$$

with $U(L)$ and $D(L)$ denoting the respective parameters of velocity and coefficient of dispersion (sometimes called diffusivity) of the travel time pdf. Let's note that Eq. (2) is also the (Hayami, 1951) solution of the Diffusive Wave

Equation (Moussa, 1997) with (U, D) standing for the mean velocity and coefficient of dispersion, respectively, of the wave flow. The influence of rainfall spatial variability on flow conditions may explain why U and D both depend on L.

The rainfall variability along flow paths can be introduced by defining the rainfall width function, as inspired from (Smith et al., 2005):

$$w_R(L,t) = \frac{R_e(L,t)}{\overline{R_e(t)}}\, w(L) \tag{3}$$

with w_R rainfall width function, and $\overline{R_e}(t)$ mean value of effective rainfall over the basin at time τ.

Unlike the width function, the rainfall width function does depend on time. (Emmanuel et al., 2015) showed that the influence of spatial rainfall variability on the basin response is well explained by the deviation between the width function and the rainfall width function associated to the pattern of rain amount during a time interval of approximately two to three times the basin response time, which is thus close to the time of concentration. The event rainfall width function w_E is defined over this duration; it was first introduced by (Woods and Sivapalan, 1999) to analyze the effect of spatial rainfall variability and runoff formation on catchment response. According to these authors, it can be assumed that the spatio-temporal variability of rainfall along flow paths can be written as the product of two independent functions, i.e.:

$$R_e\,(L,t) = w_E(L)\,\overline{R_e(t)} \tag{4}$$

with w_E event rainfall width function which depends only on hydrologic distance and $\overline{R_e}$ hyetograph of effective rainfall which depends only on time.

Introducing Eq. (4) into Eq. (1) leads to the following expression of outflow:

$$Q(t) = \int_0^{L_{max}} A\, w_E(L)dL \int_0^t R_e(L, t-\tau)\, f(L,\tau)\, d\tau \tag{5}$$

which can also be written :

$$\mathrm{Q}(t) = A \int_0^t \overline{R_e(t-\tau)}\, f_E(\tau)\, d\tau \;\; with \;\; f_E(\tau) = \int_0^{Lmax} w_E(L)\, f(L,\tau)\, dL \tag{6}$$

f_E is the E-GIUH associated with the flood event E. (Saco and Kumar, 2002a) stated that the pdf of travel time f can be approximated by replacing the varying parameters U and D by an equivalent network velocity (U_E) and equivalent hydrodynamic coefficient of dispersion (D_E), which enable preserving the mean and variance of $\boldsymbol{f_E}$. They noticed that "although used as spatially invariant parameters, they are estimated to account for the nonlinear effects that arise when varying hydrodynamic parameters".

Ultimately, the expression of E-GIUH is:

$$f_E(t) = \int_0^{L_b} \frac{L\, w_E(L)}{\sqrt{4\pi D_E\, t^3}}\, exp\left[-\frac{(L-U_E\, t)^2}{4\, D_E\, t}\right] d\tau \quad (7)$$

In addition, (Rodriguez-Iturbe and Rinaldo, 1997) found that the first two moments of f_E must satisfy the following expressions:

$$E(T) = \frac{1}{U_E}\, E(L)\ and\ Var(T) = 2\, \frac{D_E}{U_E^2}\, E(L) + \frac{1}{U_E^2}\, Var(L) \quad (8)$$

where $E(L)$ and $Var(L)$ are the first two moments of the pdf of hydrological paths.

In sum, the spatial variability of rainfall can be integrated into the width function-based GIUH by replacing the width function by the rainfall width function. This formulation paves the way to determining the E-GIUH, which characterizes the basin response to each rain event forcing.

2.2 Principles of the E-GIUH identification process

The problem posed consists of identifying the E-GIUH, specific to flood event E that leads to the best reconstitution of the observed hydrograph at the basin outlet. This E-GIUH is defined by two parameters U_E and D_E as well as by the event rainfall width function w_E. Note that Equation (6) expresses the hydrograph as a function of both E-GIUH and the hyetograph of effective rainfall, meaning that the identification of effective rainfall and Event-GIUH are not independent of one another and moreover that the transformation of observed rainfall data fields into a hyetograph of effective rainfall might influence the identified E-GIUH. For this reason, the components of the hyetograph of effective rainfall are also considered as parameters. Nevertheless, the adopted identification algorithm (Section 4) provides the opportunity to introduce the hyetograph of effective rainfall as an "*a priori*" information to which a level of confidence is ascribed, thus making it possible to control its influence on the result. Lastly, the E-GIUH identification process calls for a model capable of combining the following equations:

i) Flow at the catchment outlet expressed as the convolution product: $Q = \overline{R_e} * f_E(U_E, D_E)$, written in a discretized manner:

$$Q_j = A\, \sum_{k=1}^{k=j} \overline{R_e}_{j+1-k}\, f_{E_k}(U_E, D_E) \quad (9)$$

with:

$$f_{E_k}(U_E, D_E) = \sum_{\gamma=1}^{\gamma=n_w} w_{R\gamma} \int_{(k-1)\Delta t}^{k\,\Delta t} \frac{\bar{L}_\gamma}{\sqrt{4\pi D_E\, \tau^3}}\, exp\left[-\frac{(\bar{L}_\gamma - U_E \tau)^2}{4 D_E\, \tau}\right] d\tau \quad (10)$$

where: $\boldsymbol{Q} = \left(Q_1, Q_2, \ldots . Q_{m_q}\right)$ is the vector grouping the $m_q$components of the event hydrograph, $\overline{\boldsymbol{R_e}} = (\overline{R_e}_1, \overline{R_e}_2, \ldots\ldots, \overline{R_e}_{m_r})$ the vector grouping the m_r components of the hyetograph of effective rainfall over the basin,

and $\boldsymbol{w_E} = (w_{E1}, w_{E2}, \ldots\ldots w_{En_w})$ the vector grouping the n_w components of the event rainfall width function at distances $(L_1, L_2, \ldots. L_{n_w})$. The vector $\boldsymbol{f_E} = (f_{E_1}, f_{E_2}, \ldots. f_{E_{m_f}})$ regroups the m_f components of the E-GIUH.

ii) A conservation equation stating that runoff volume at the outlet amounts to the effective rainfall:

$$\sum_{k=1}^{k=m_q} Q_k = A \sum_{k=1}^{k=m_r} \overline{R_e}_k \quad (11)$$

iii) The discretized form of Equations (8), which relate the parameters of the E-GIUH with the pdf of hydrological distances, in the framework of GIUH theory:

$$E(T, U_E, D_E) - \frac{\bar{L}}{U_E} = 0 \quad (12)$$

$$Var(T, U_E, D_E) - 2\,\frac{D_E}{U_E^3}\,\bar{L} + \frac{1}{U_E^2}\,V(L) = 0 \quad (13)$$

with:

$$\bar{L} = \sum_{\gamma=1}^{\gamma=n_w} w_{E\gamma}\, L_\gamma \; and \; V(L) = \sum_{\gamma=1}^{\gamma=n_w} w_{E\gamma}\left[L_\gamma - \bar{L}\right]^2 \quad (14)$$

Moreover, the vector of parameters to identify is: $\boldsymbol{p} = (U_E, D_E, \overline{\boldsymbol{R_e}})$, while the vector grouping the data associated with Equations 9, 11, 12 and 13, used to base the identification procedure is: $\boldsymbol{d_0} = (\boldsymbol{Q_0}, \sum_{k=1}^{k=m_r} Q_{0k}, 0.0, 0.0)$.

3. Case study and dataset

The Cevennes Region encompasses a medium-elevation mountain range located in the southeastern part of France's Massif Central sector (Fig. 1). The southeastern end of this range consists of a plateau and a plain area extending to the Mediterranean Coast. Several rivers originate in the Cevennes Mountains and cross the intermediate plain to empty into the Rhone River or flow into the Mediterranean Sea. This region displays typical Mediterranean climate and is subject to heavy rainfall events during the fall, causing flash floods that can result in considerable damage and losses. The Cevennes Region is covered by a network of rain gauges at a density of roughly 1 gauge every 150 km^2, complemented by two weather radars that provide quantitative precipitation estimates (QPE) at a high spatial (1 km x 1 km) and temporal (5 min) resolution. Hydrometeorological recordings in this region are enhanced by the presence of the OHMCV (Cevennes-Vivarais Mediterranean Hydrometeorological Observatory) (http://www.ohmcv.fr). This long-term observatory has built an integrated hydrometeorological database of flash flood events across the Cevennes-Vivarais area. The available operational datasets have therefore undergone a thorough quality control and can be considered highly accurate (Boudevillain et al., 2011). The OHMCV provides several QPE products. For purposes of this study, the hourly rainfall fields of

1 km x 1 km spatial resolution, obtained by means of a radar - rain gauge merging technique proposed by (Delrieu et al., 2014) have been used; these fields offer a high level of accuracy compared to other QPE products.

The basins considered herein are: Gard at the Anduze gauging station (surface area: 545 km²), and Ardèche at the Vogüe gauging station (620 km²). Upstream of Anduze, the Gard bedrock consists mainly of schist (61%) and granite (18%). The Ardèche bedrock upstream of Vogüe is mostly granitic (72%) (Douinot et al., 2018). The hydrographic network of these two basins has been determined with the TauDem tool (Tarboton, 1997), in using a DTM at a spatial resolution of 250 m. Both basins are well documented and have been the subject of several works on rainfall-runoff modeling (Adamovic et al., 2015; Douinot et al., 2018; Moussa et al., 2007; Naulin et al., 2013; Saulnier and Le Lay, 2009; Tramblay et al., 2011; Vannier et al., 2016) and flash flood forecasting (Alfieri et al., 2011; Dolcine et al., 2001).

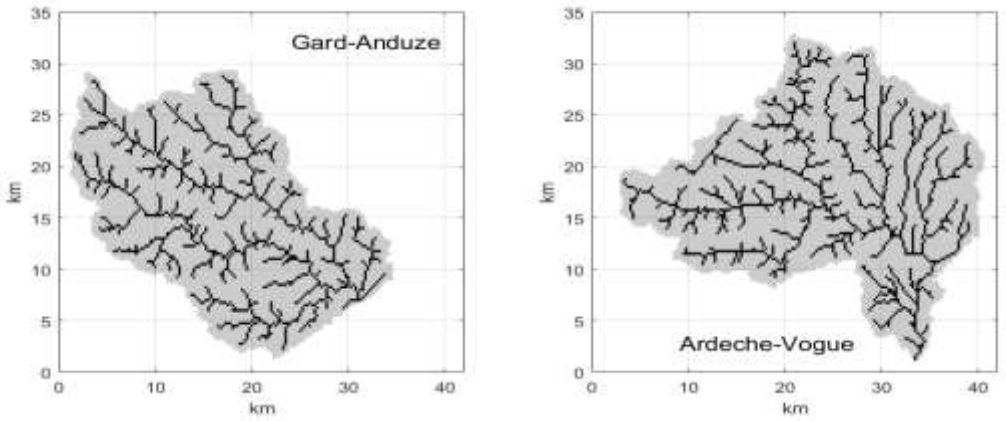

Figure 1: Case study of the two basins studied

The QPE product covers a time period from 2011 to 2014 and includes one very intense and significant rain event in September 2002 (Delrieu et al., 2005). A sample of six flood events at each basin have been selected, comprising both rain and flow data. All these events are single-peak hydrographs, which are more easily adapted to characterizing a unit hydrograph. Some selected events occurred during long rainy periods, which explains the high flow values observed upon their initiation. The main features of these flood events are summarized in Table 1. The peak flow of a two-year return period is, respectively, Q2 = 630 m^3/s for Gard-Anduze and Q2 = 740 m^3/s for Ardèche-Vogüe, thus indicating that the dataset contains flow events of various magnitudes. The coefficient of variation in the spatial rainfall amount ranges from 0.08 to 1.04 for Gard-Anduze and from 0.22 to 0.76 for Ardèche-Vogüe, which confirms the varied characteristics of the selected flood events.

Basin	Flood Event		Peak flow (m^3/s)	Rainfall duration (h)	Rainfall amount (mm)	Rainfall variability (coef. var)
Gard (Anduze) 545 km^2	G1	Oct 8-9, 2002	2,744	23	294.6	0.44
	G2	Oct 20-23, 2008	933	10	125.8	1.04
	G3	Oct 31 - Nov 3, 2008	1,010	61	287.8	0.25
	G4	Oct 29 - Nov 1, 2010	306	41	191.1	0.08
	G5	Sept 17-21, 2014	1,010	25	148.8	0.50
	G6	Nov 14, 2014	616	17	98.9	0.38
Ardèche (Vogüe) 620 km^2	A1	Oct 20-23, 2008	953	26	158.6	0.31
	A2	Oct 31 - Nov 3, 2008	983	44	169.3	0.76
	A3	Sept 6-8, 2010	1,270	30	225.1	0.22
	A4	Dec 21-24, 2010	571	56	153.6	0.22
	A5	Oct 22-25, 2013	850	28	126.1	0.27
	A6	Oct 9-15, 2014	1,090	48	181.4	0.66

Table 1: Characteristics of the selected flood event

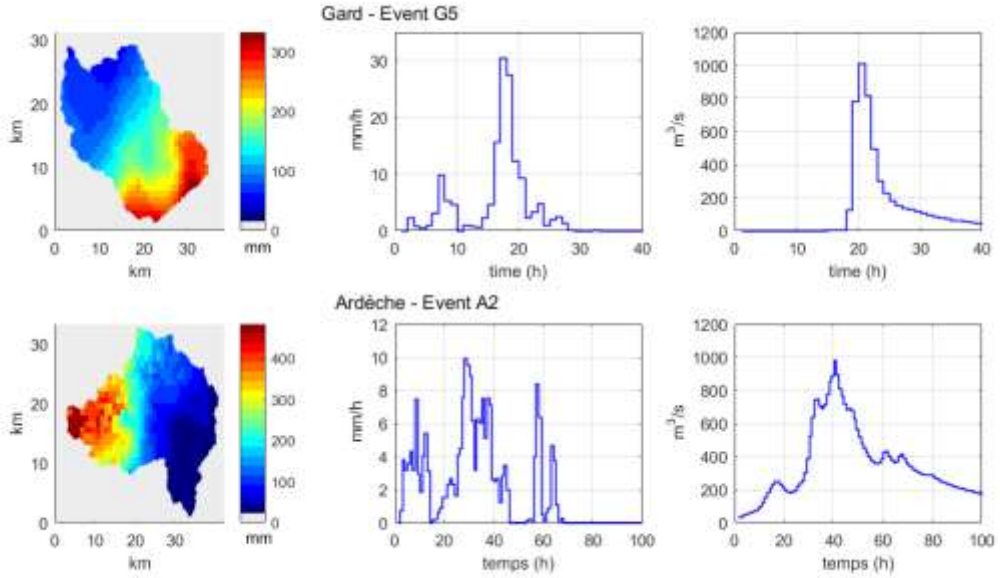

Figure 2: Examples of flood events – Map of total rainfall (left) – Hyetograph (center) – Hydrograph (right)
(The 12 flood events of the data set are displayed in supplementary material)

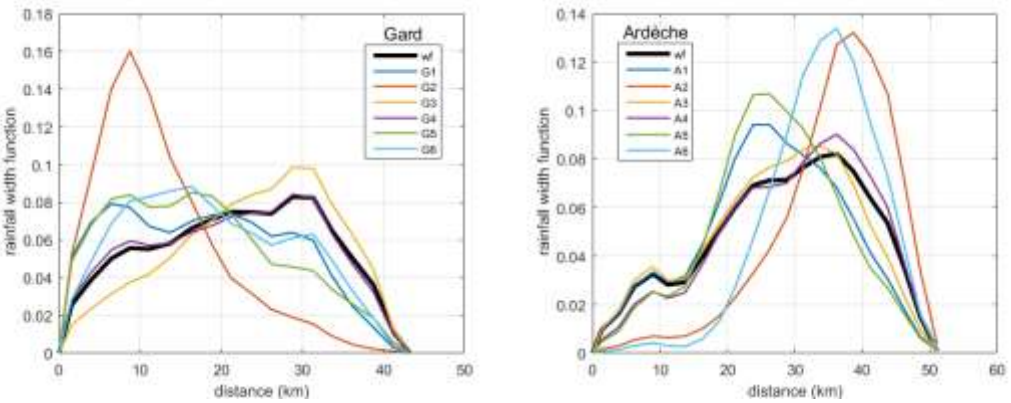

Figure 3: Rainfall width functions of the studied flood events - the left graph combines the six Gard-Anduze Basin events and the right graph the Ardèche-Vogüe Basin event. The thick black continuous line provides the width function of each basin.

Figure 2 illustrates one event for each basin: G5 for Gard A2 for Ardèche. The other events of each basin are displayed in the Supplementary Information section. It can be noted that the rainfall map of Event G5 indicates that the maximum rainfall occurs downstream, as confirmed by the corresponding rainfall width function shown in Figure 3 (left graph). The rainfall map of Event A2 is quite different, with the maximum rainfall being located upstream, which has been clearly confirmed by the associated rainfall width function (Fig. 3, right graph). The rainfall width functions presented in Figure 3 reveal that most rain events feature significant variability along the hydrological path, and moreover the events of the two basins are of a different nature. For Gard-Anduze (left graph), all events but one are characterized by a higher rainfall amount downstream, while for Ardèche-Vogüe most rain events are characterized by a higher rainfall amount upstream or in the central part of the basin. It is clear that these rainfall features can influence the basin response to rainfall forcing, along with the E-GIUH summarizing this response.

4. Application and results

4.1 The identification algorithm

It has been proposed to treat E-GIUH identification within the framework of inverse theory, as detailed in the textbooks by (Menke, W. 2012; Tarentola, A., 2005).

The solution minimizes the following expression:

$$\Phi(\boldsymbol{d},\boldsymbol{p}) = [\boldsymbol{m}(\boldsymbol{d}) - \boldsymbol{d}]^t \, \boldsymbol{C}_Q^{-1} \, [\boldsymbol{m}(\boldsymbol{p}) - \boldsymbol{d}_0] + [\boldsymbol{p} - \boldsymbol{p}_0]^t \, \boldsymbol{C}_P^{-1} \, [\boldsymbol{p} - \boldsymbol{p}_0] \quad (15)$$

$$\boldsymbol{d} = m(\boldsymbol{p})$$

where: Φ is the likelihood function, t signifies transpose, *m* denotes the model relating data and parameters, $\boldsymbol{p}_0$ is the vector of *a priori* parameters, $\boldsymbol{C}_p$ is the covariance matrices of residuals between truth (and unknown) and *a priori* parameters, and $\boldsymbol{C}_{dm}$ the covariance matrix combining data and modeling uncertainties (Tarentola, A., 2005).

The statistical distributions of both $[\boldsymbol{d} - \boldsymbol{d}_0]$ and $[\boldsymbol{p} - \boldsymbol{p}_0]$ are assumed to be unbiased and Gaussian. Menke (1989) demonstrated that the solution vector $\boldsymbol{p}'$ satisfies:

$$\boldsymbol{p}' = \boldsymbol{p}_0 + \boldsymbol{C}_p \boldsymbol{M}^t \left[\boldsymbol{M}^t \boldsymbol{C}_p \boldsymbol{M} + \boldsymbol{C}_{dm}\right]^{-1} [\boldsymbol{d}_0 - m(\boldsymbol{p}') + \boldsymbol{M}(\boldsymbol{p}' - \boldsymbol{p}_0)] \quad (16)$$

where $\boldsymbol{M}$ is the matrix of (first-order) partial derivatives of model *m*. If model *m* is nonlinear, (Tarentola, A., 2005) demonstrated that the solution can be obtained using a quasi-Newton method by means of the following algorithm (Equation 3.51, p. 69):

$$\boldsymbol{p}_{n+1} \approx \boldsymbol{p}_n - \mu_n \left[\boldsymbol{M}_n^t \boldsymbol{C}_p^{-1} \boldsymbol{M}_n + \boldsymbol{C}_d^{-1}\right]^{-1} \left[\boldsymbol{M}_n^t \boldsymbol{C}_{dm}^{-1} \langle m(\boldsymbol{p}_n) - \boldsymbol{d}_0 \rangle + \boldsymbol{C}_p^{-1} \langle \boldsymbol{p}_n - \boldsymbol{p}_0 \rangle\right] \quad (17)$$

in which $\boldsymbol{P}_n$ constitutes the result of the nth iteration, $\boldsymbol{M}_n = \frac{\partial\, \boldsymbol{m}(\boldsymbol{p}_n)}{\partial(\boldsymbol{p}_n)}$ is the matrix of (first-order) partial derivatives of the model at point $\boldsymbol{p}_n$, and $\mu_n < 1$ serves to control the convergence. More information regarding the resolution of such nonlinear problems can be found in (Menke, 2012; Tarentola, A., 2005).

The *a priori* information, introduced in terms of $(\boldsymbol{p_0}, \boldsymbol{C}_p)$, contains the initial knowledge of the parameters to be identified, along with the confidence ascribed to this knowledge. If the observed data are insufficient or if the level of confidence in the data is low, then the problem becomes underdetermined and the *a priori* information assumes a dominant role. If the problem is over-determined (i.e. availability of very high quality data in sufficient quantity), the solution would only depend very little on the *a priori* information.

The next section presents the application conditions of this inverse algorithm in order to identify the E-GIUH by focusing on the *a priori* information that initializes the identification process.

4.2 Identification algorithm – A priori information

4.2.1 Data and associated covariance matrix

The data vector, which regroups $n_d = m_q + 3$ components, $\boldsymbol{d_0} = (\boldsymbol{Q_0}, \sum_{k=1}^{k=m_r} Q_{0k}, 0.0, 0.0)$, was introduced in Section 2.2. Its covariance matrix $\boldsymbol{C}_{dm}$ characterizes the uncertainties on both the data and model equations.

This matrix is assumed to be diagonal, and the standard deviations associated with both the data and model equations have been assembled in the vector $\boldsymbol{\sigma_{d_0}} = \left(\boldsymbol{\sigma_{Q_0}}, \sigma_{\Sigma Q_0}, \sigma_E, \sigma_V\right)$, with:

$$\boldsymbol{\sigma_{Q_0}} = \left(\sigma_{Q_1}, \ldots\ldots, \sigma_{Q_{m_q}}\right) \; and \; \sigma_{Q_{0i}} = \; max\left[\; \alpha_Q \; Q_{0i}, \sigma_{Q_{min}}\right] \tag{17}$$

$$\sigma_{\Sigma Q_0} = \alpha_\Sigma \left[\sum_{k=1}^{k=m_q} Q_k\right]$$

$$\sigma_E = \; \alpha_E \; E(T, U_e, D_e)$$

$$\sigma_V = \; \alpha_V \; Var(T, U_e, D_e)$$

$\alpha_\Sigma, \alpha_E, \alpha_V$ are the coefficients of variation of the errors associated with Equations (11), (12) and (13), respectively.

4.2.2 A priori E-GIUH parameters

The two E-GIUH parameters are velocity (U_E) and the coefficient of dispersion (D_E). Nevertheless, the E-GIUH components also depend on the event rainfall width function ($\boldsymbol{W_E}$), which reveals the spatial pattern of effective rainfall. The rainfall width function is derived from radar time series data; let's note that this choice is associated with the measured rainfall width function and not the effective rainfall width function. Such caution is exercised in seeking to maintain the E-GIUH independent of the *a priori* effective rainfall, which may be erroneous. Comparison tests conducted between rainfall width functions and effective rainfall width functions, by means of the Kolmogorof-Smirnov protocol, have confirmed that the two pdfs are not significantly different.

The *a priori* velocity (U_{E0}) and *a priori* hydrodynamic coefficient of dispersion (D_{E0}) are both set by the user and accompanied by their standard deviations of σ_U and σ_D, respectively.

The total coefficient of dispersion of the GIUH is expressed as follows (Rodriguez-Iturbe and Rinaldo, 1997):

$$D_{G0} + \; D_{E0} \; = \; \frac{U_{E0}^2 \, Var(T)}{2 \, L} \; and \; D_{G0} = \frac{U_{E0} \, Var(L)}{2 \, L} \tag{18}$$

4.2.3 A priori parameters: Hyetograph of effective rainfall $\boldsymbol{R_e}$

The GIUH expresses the transformation of effective rainfall over the basin to flow at its outlet. It is worth considering the accuracy of effective rainfall. The hydrograph of effective rainfall is incorporated into the parameters of the inverse algorithm and moreover defined by its *a priori* components ($\boldsymbol{R_{n0}}$) as well as the associated error covariance matrix. The inverse algorithm offers a flexibility that enables taking the effective rainfall into account in various ways, ranging between two extreme situations, namely:

i) the basin production function, giving rise to a vector grouping the *a priori* hyetograph of effective rainfall components ($\boldsymbol{R_{e0}}$), is considered to be accurate, and the associated covariance terms are very weak. The inverse algorithm does not significantly modify the *a priori* hyetograph of effective rainfall, and its functioning is nearly the equivalent to the calibration of the two parameters defining the E-GIUH;

ii) the production function is unknown, and the hyetograph of effective rainfall components are the parameters to be determined. In this case, ($\boldsymbol{R_{e0}}$) is not considered to be accurate, and the associated covariance terms are assigned large values. The inverse algorithm identifies both the net hyetograph and E-GIUH and moreover may be viewed as an evolution of the method developed by (Duband et al., 1993) to simultaneously identify the unit hydrograph common to all events and the hyetograph of effective rainfall of each of them.

The matrix of error covariance of the effective rainfall hyetograph is defined as follows:

$$cov\left(R_{e0i}, R_{e0j}\right) = \sigma_{Ri}\,\sigma_{Rj}\,\exp\left[-\left(\frac{|i-j|\Delta t}{T_R}\right)^2\right] \;\; with\;\sigma_{R\,i} = \; max\;\left(\alpha_R R_{e0i}, \sigma_{Rmin}\right) \tag{19}$$

with *i* and *j* being time indices, $\sigma_{R\,i}$ and $\sigma_{R\,j}$ the error standard deviation of R_{e0i} and R_{e0j}, respectively. α_R is the coefficient of variation in the error characterizing the hyetograph of effective rainfall, β_R denotes the minimum value assigned to the error standard deviation, and T_R is the decorrelation time controlling the temporal structure of the errors affecting successive components of the *a priori* net hyetograph.

The role of the *a priori* net hyetograph in the E-GIUH identification is defined by the value assigned to α_R. A very weak value, e.g. 0.05, means that the *a priori* net hyetograph is assumed to be highly accurate, whereas a larger value, e.g. 0.2 to 0.3, indicates that the *a priori* net hyetograph is assumed to be inaccurate.

4.3 Reference E-GIUHs

4.3.1 Data and model description

The flow data are assumed to be of good quality. The coefficient of variation of the flow measurement error has been set at $\alpha_Q = 0.10$, with a minimum value of $2m^3s^{-1}$. Equation (9) is assumed to be exact and free of any error. Equation (11), which expresses the budget equation and is assumed to be associated with a weak error characterized by its small coefficient of variation, $\alpha_\Sigma = 0.05$. The theoretical GIUH framework coupled with the introduction of the spatial rainfall variability accurately depicts the true E-GIUH (Equations 12 and 13). This modeling error is then defined by weak coefficients of variations: $\alpha_E = 0.05$ and $\alpha_V = 0.05$, respectively.

4.3.2 A priori E-GIUH

A constant *a priori* velocity has been adopted for all flow events of the same basin. The standard deviation values retained are $\sigma_U = 0.5ms^{-1}$ and $\sigma_D = 1000\, m^2s^{-1}$, in order to leave a wide interval of variation with respect to the *a priori* values. The *a priori* E-GIUH also depends on the rainfall width function w_{E0}, which has been derived from radar time series data. Let's note once again that this choice is associated with the measured rainfall width function and not the effective rainfall width function. Such an exercise of caution aims to maintain the E-GIUH independent of the *a priori* effective rainfall, which may be erroneous. In addition, the comparison of rainfall width functions and effective rainfall width functions for these case study events, by means of the Kolmogorof-Smirnov test, have confirmed that they do not differ significantly.

The SCS model has been adopted to provide the *a priori* values of the net hyetograph. This classical model is widely used, and recent tools have been developed to derive the curve number values from remote sensing data (Ross et al., 2018; Zeng et al., 2017). The SCS model has been successfully applied to basins subject to flooding in this Mediterranean region (Naulin et al., 2013). It is being used herein by considering a parameter, S_{moy}, that represents the mean storage capacity of the basin for a given event. The runoff volume is defined by:

$$Vr = \sum_{k=1,p} \frac{(Rt_k - Ia_k)^2}{(Rt_k - Ia_k) + S_k} \quad (20)$$

with Vr denoting the runoff volume at the basin outlet, p the number of meshes in the basin grid, Rt_k the rainfall amount, S_k the storage capacity, and $Ia_k = 0.2\, S_k$ the initial loss of mesh *k*. The CN values are then transformed into a map of relative storage capacity, from which the storage capacity of each mesh is derived: $S_k = S_{moy}\, \gamma_k$, with γ_k being the relative storage capacity of mesh *k*. S_{moy} has been calibrated for each flood event so that the effective rainfall volume is equal to the runoff volume. As runoff generated by the effective rainfall is assumed to be the dominant process of flow generation, the base flow is removed from the observed flow values. The pre-event base flow is the measured flow at the beginning of the rain event. At the end of the event, it is assumed that the runoff contribution becomes negligible after the rain has stopped for a period equal to the basin time of concentration. The post-event base flow is the flow measured at this time. It is assumed that the base flow varies linearly between these values during the flood event. The time of concentration is estimated to be 18h for the Gard-Anduze basin and 24 h for the Ardèche-Vogüe basin. Changing the concentration times by a few hours don't significantly affect the obtained results.The net hyetograph ($\boldsymbol{R_{e0}}$) is thus deduced from the time series of hourly effective rainfall maps.

For the identification of the reference E-GIUH, it is assumed that the *a priori* effective rainfall is highly accurate. The coefficient of variation of each net hyetograph component is then given by the value α_R = 0.10. In addition, $T_R = 2\ h$ controls the temporal structure of the error on the *a priori* net hyetograph.

The application conditions selected to derive the reference E-GIUHs are collated in Table 2

Hydrological distance increment: $\Delta L = 2500\ m$
Data and model errors:
Error on flow: $\alpha_Q = 0.10$ Conservation of flux – Eq. (17): $\alpha_\Sigma = 0.05$ E-GIUH equation – Eq. (17): $\alpha_E = 0.05$ E-GIUH equation – Eq. (17): $\alpha_V = 0.05$
A priori parameter values:
Velocity: $U_{E0} = 1.2\ ms^{-1}$ (Gard-Anduze), $U_{E0} = 1.0\ ms^{-1}$ (Ardèche-Vogüe), $\sigma_U = 0.5 ms^{-1}$ Coef. of dispersion provided by Eq. (18) $D_{E0} \approx D_{G0}/2$ and $\sigma_D = 1200\ m^2 s^{-1}$ *A priori* net hyetograph: SCS - α_R = 0.10 and $T_R = 2\ h$

Table 2: Summary of the reference applications conditions

4.4 Results and discussion

The accuracy of the identified E-GIUH can only be evaluated indirectly. The classical Nash-Sutcliffe efficiency criterion (denoted NSE) is used for such a purpose:

$$NSE_x = 1 - \frac{\sum_{i=1}^{i=n}(x_{ref\ i} - x_{tes\ i})^2}{\sum_{i=1}^{i=n}(x_{ref\ i} - \bar{x})^2} \quad (21)$$

with $[x_{ref\ i}]$ reference vector of *n* components of mean $\overline{x_{tes}}$, $[x_i]$ vector to be tested.

The E-GIUHs identified according to the reference application conditions are displayed in Figure 4.

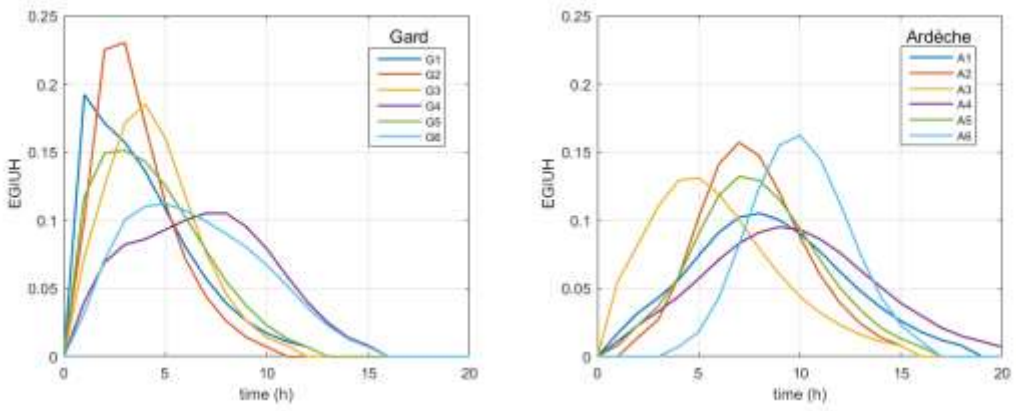

Figure 4: Identified Event-GIUHs relative to the reference application conditions

These results have been assessed by calculating four criteria: 1) NSE_Q between observed hydrographs and hydrographs modeled using *a priori* E-GIUH and an *a priori* net hyetograph; 2) NSE_Q between observed hydrographs and hydrographs modeled using the identification results; 3) NSE_{Rn} between the *a priori* net hyetograph and the identified net hyetograph; and 4) NSE_{GIUH} between the *a priori* E-GIUH and the identified E-GIUH. These criteria are calculated for each flood event; their average value is computed for the two basins so as to provide an overview of the results obtained. These criteria have been compiled in Table 3, leading to the following comments:

- The identified E-GIUHs allow improving the simulation of observed hydrographs. This improvement seems as more pronounced as the identified values of (U_E, D_E) differ from the *a priori* values. The average increase in NSE_Q is significant, from 0.72 to 0.83 for Gard-Anduze and from 0.65 to 0.84 for Ardèche-Vogüe.

- This increase primarily results from an evolution in E-GIUHs. Indeed, a comparison of the net hyetographs indicates that the *a priori* ones slightly differ from the identified ones. The average value of NSE_{Rn} equals 0.97 for Gard-Anduze and 0.96 for Ardèche-Vogüe; in all cases, the criterion is above 0.92.

- A comparison of the *a priori* and identified E-GIUHs confirms quite well that based on the reference conditions, the identification method acts primarily on E-GIUHs. Indeed, the average values of NSE_{GIUH}, 0.74 for Gard-Anduze and 0.65 for Ardèche-Vogüe, underscore that *a priori* E-GIUHs differ considerably from identified ones.

Beyond these criteria, it is very interesting to note the wide diversity and wide variability of the E-GIUHs of each basin. For instance, the time to peak for Gard-Anduze flood events (left graph) ranges from one hour to seven hours, while the time to peak for Ardèche-Vogüe flood events ranges from 5 to 10 hours. These results confirm not only the influence of rainfall variability on the E-GIUH, but also the fact that the E-GIUH could be well adapted to serve as a signature characteristic of a flood event.

Basin	Flood event	*A priori* parameters		Identified parameters		Evaluation criteria			
		U_{E0} (m/s)	D_{E0} (m²/s)	U_E (m/s)	D_E (m²/s)	1 NSE_Q *A priori*	2 NSE_Q Identified	3 NSE_{Rn}	4 NSE_{GIUH}
Gardo (Anduze) 545 km²	G1	1.2	1,700	1.54	5,180	0.77	0.83	0.92	0.72
	G2	1.2	1,219	1.24	958	0.86	0.88	0.99	0.99
	G3	1.2	1,129	1.78	4,209	0.73	0.92	0.99	0.06
	G4	1.2	1,476	1.03	873	0.51	0.75	0.97	0.87
	G5	1.2	1,693	1.47	2,323	0.69	0.75	0.97	0.90
	G6	1.2	1,464	0.93	1,000	0.76	0.92	0.96	0.83
	Average	1.2	1,447	1.33	2,425	0.72	0.84	0.97	0.73
Ardèche (Vogüe) 620 km²	A1	1.0	970	1.00	1,548	0.80	0.89	0.96	0.98
	A2	1.0	493	1.45	2,605	0.71	0.94	0.97	-0.31
	A3	1.0	1,059	1.36	4,330	0.50	0.79	0.93	0.33
	A4	1.0	937	0.96	1,540	0.80	0.87	0.99	0.97
	A5	1.0	768	1.13	1,460	0.64	0.85	0.93	0.87
	A6	1.0	383	1.09	652	0.46	0.77	0.92	0.90
	Average	1.0	768	1.17	2,022	0.65	0.85	0.95	0.63

Table 3: Results for the 12 studied events – Comparison of *a priori* and final parameters and evaluation criteria

The *a priori* values of the E-GIUH parameters (U_{E0}, D_{E0}) have been chosen regardless of the event features. What conclusions can be drawn from their resulting values? For the sake of simplicity, the hydrological features of a flood event are summarized by its specific flow peak (q_{max}), considered as an indicator of the event magnitude. The use of a specific flow peak allows regrouping the events of both catchments on the same graph in order to study a possible relationship between this indicator and the E-GIUH parameters. The scattergrams (U_E, q_{max}) and (D_e, q_{max}) with q_{max} as the specific flow peak are displayed in Figure 5. It can be observed that a significant correlation exists between the two E-GIUH parameters and the specific flow peak. Let's note that the coefficient of determination (R^2) has been calculated without accounting for the exceptional flow event that occurred on Sept 20-21, 2002. The limited size of the dataset and the fairly low value of R^2 do not offer the basis for a more detailed analysis. This result however could suggest that:

- The mean flow velocity U_E increases with the magnitude of the flood event, which appears to be logical and consistent with previous results. It is interesting to note that taking the rainfall width function into consideration does not alter this mean trend, even though it could be surmised that flood events displaying a strong rainfall variability also exhibit a stronger variability in flow velocity within the hydrological network.

- Results regarding the coefficient of dispersion D_E are not simple to analyze. The model equations relate D_E and U_E, which would contribute to the link between q_{max} and D_E. Similarly, the average values of D_E and U_E (Table 2) indicate a strong increase in D_E values with respect to the *a priori* values, thereby likely to generate an accurate restitution of the observed hydrographs. Lastly, the sensitivity study (next section) suggests that this identification procedure is not highly sensitive to D_E. Moreover, it is not yet possible to draw a clear conclusion, and studying a larger sample of events would allow progressing in this effort.

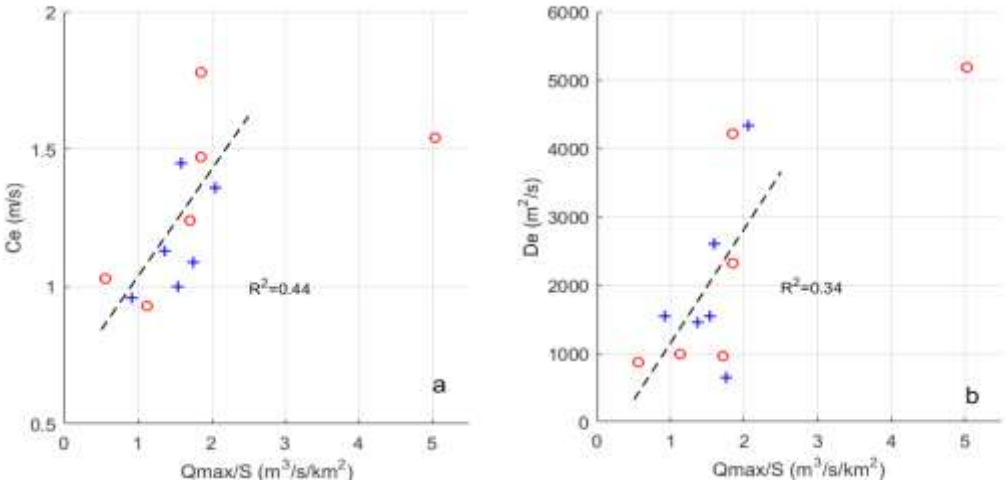

Figure 5: Relationship between the specific peak flow and the E-GIUH parameters of the flood events

4.5 Sensitivity study of the E-GIUH identification

This sensitivity study addresses the influence of the application conditions on the identified E-GIUHs. This section provides the main results and conclusions of the sensitivity study; a detailed presentation can be found in the Supporting Information. Note that special attention has been paid to the influence of the *a priori* hyetograph of effective rainfall.

4.5.1 Sensitivity to (U_E, D_E) variations

This test examines the influence of (U_E, D_E) variations on the simulated E-GIUHs and hydrographs. The E-GIUHs and hydrographs obtained by varying (U_E, D_E) values with respect to the reference solution are compared to the E-GIUHs and hydrographs of this reference solution by calculating the NSE values. Figure 5 illustrates the results of this test, which yields two key indications: i) the influence of D_E is much weaker than that of U_E; and ii) the simulated hydrographs are much less influenced by (U_E, D_E) variations than the simulated E-GIUHs. This latter result proves to be important, given that the identification procedure is mostly based on observed

hydrographs. This sensitivity study confirms that a reliable estimation of (U_E, D_E) from hydrographs is far from being straightforward.

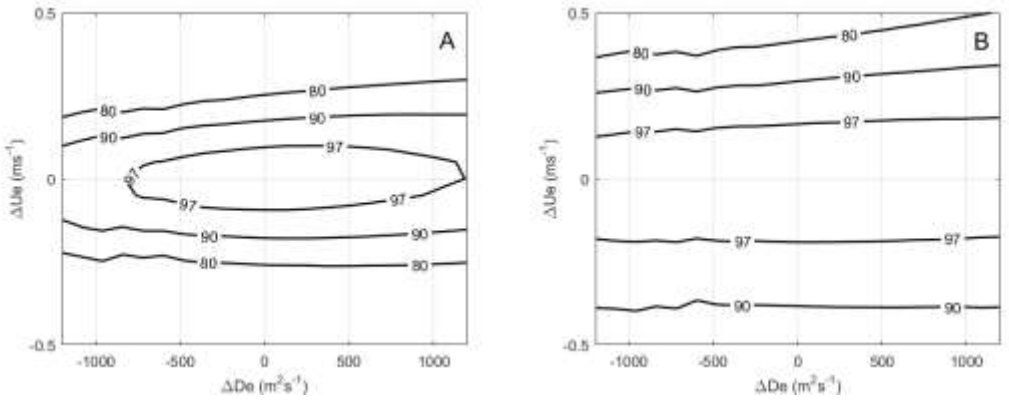

Figure 6: Sensitivity of E-GIUHs (A) and simulated hydrographs (B) to variations in (U_E, D_E)

4.5.2 Sensitivity of the E-GIUH to inverse algorithm application conditions

This part of the sensitivity study comprises: i) the confidence assigned to flow data (coefficient of variation α_Q), ii) the confidence assigned to the GIUH theoretical model (coefficients of variation α_E and α_V), iii) the influence of the *a priori* value of D_{E0}, iv) the influence of the *a priori* value of U_{E0}, and lastly v) the confidence assigned to the *a priori* hyetograph of effective rainfall (coefficient of variation α_R). It is performed by running the E-GIUH identification in varying one of these factors with respect to the reference conditions. The results obtained are summarized in Table 4 and then detailed in the Appendix.

It is interesting to emphasize the influence of an increase of α_R which controls the error variance on the *a priori* hyetograph of effective rainfall. It is confirmed that an increase of α_R results in an improvement of the restitution of the observed hydrograph. The overall improvement is obtained by changes in the resulting effective rainfall hyetograph, thus confirming the capability of this method to identify both the E-GIUH and the hyetograh of effective rainfall (Rn). This result might extend the application domain of the proposed method, but this subject is out the scope of the present work which focuses on the identification of E-GIUHs.

Variable	Sensitivity of the identification result	Comment
α_Q	Strong	Decrease in NSE_Q as α_Q increases.
α_E, α_V	Weak	Significant increase in the mean value of D_E as both α_E and α_V increase.
D_{E0}	Weak	Increase in the mean value of D_E as D_{E0} increases. This result is consistent with the previous section.
U_{E0}	Moderate	An *a priori* underestimation seems to be more detrimental than an overestimation. A conservative *a priori* value seems to be preferable.
α_R	Moderate to strong	The increase in α_R results in an increase of NSE_Q. The identified E-GIUHs are only slightly affected. The overall improvement is obtained by changes in the resulting effective rainfall hyetograph.

Table 4: Conclusions drawn from the sensitivity study

4.5.3 Influence of the a priori hyetograph of effective rainfall

The previous results have been obtained by considering that the widely used SCS production function accurately represents basin operations. The question raised then is whether the choice of an *a priori* hyetograph of effective rainfall affects the identified E-GIUHs. This test is conducted by running the method with an *a priori* hyetograph of effective rainfall that's very different from the SCS one, so as to introduce a sharp contrast with the reference application conditions. The selected production function (denoted CR-PI) assumes initial losses of 20 mm in each mesh of the basin, along with a constant runoff coefficient. For each flood event, this coefficient is estimated such that the effective rainfall volume is equal to the runoff volume. The choice of the *a priori* net hyetograph is the only modification adopted with respect to the reference application conditions. The two *a priori* net hyetographs are assumed to be rather inaccurate, with an error covariance α_R = 0.25. It then becomes possible to compare the E-GIUHs identified based on the SCS and CR-PI production function, respectively. The *a priori* E-GIUHs turn out to be similar for both cases. The comparison results are detailed in the Supporting Information section and illustrated in Figure 6, which displays the 12 E-GIUHs obtained from the SCS (continuous line) and the CR-PI (dashed line) net hyetographs, respectively. The reference E-GIUH (thin continuous line) has been added to this comparison. The sensitivity test shows that for 9 of the 12 flood events, the identified E-GIUH is very weakly affected by the change in *a priori* net hyetograph ($NSE_{GIUH} > 0.94$), only moderately affected for 2 of them ($NSE_{GIUH} = 0.88$) and significantly affected for 1 other event (A1-$NSE_{GIUH} = 0.80$). More specifically,

Figure 7 indicates that the differences between the 12 E-GIUHs remain quite pronounced and much larger than the fluctuations of each E-GIUH. In addition, it is confirmed that the identification method serves to improve the net hyetograph, with the identified ones lying much closer than the *a priori* ones.

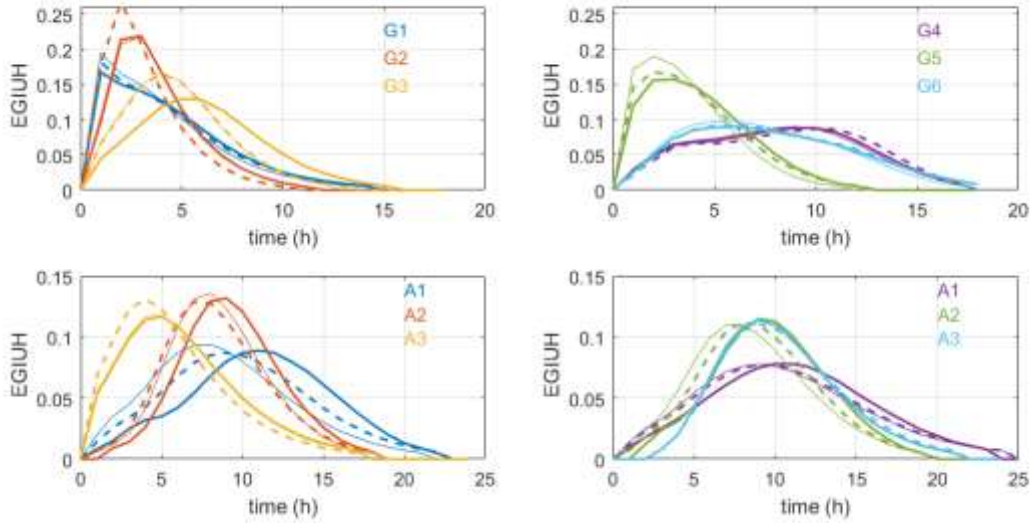

Figure 7: Sensitivity of the E-GIUHs to the production function (SCS and Cr-PI). For each of the 12 flow events, three E-GIUH of the same color are displayed: E-GIUH obtained with the SCS (αR = 0.25; plain line); E-GIUH obtained with CR-PI (αR =0.25; dashed line); reference (thin line). The two upper graphs are for Gard-Anduze and the lower for Ardèche-Vogüe

5. Summary and conclusion

The GIUH has become a classical representation of the rapid response of a basin when adapted to rainfall-runoff modeling. If the GIUH depends on the morphological features of a basin, then it is also influenced by the characteristics of rainfall patterns as well as by the variability of flow path velocities. We have therefore considered that an Event-specific GIUH (or E-GIUH) exists that actually characterizes the catchment response under the specific conditions of each flood event. The method proposed herein to identify this E-GIUH relies on the width function-based GIUH (Rigon et al., 2016), as adapted to take into account the spatial variability of rainfall through replacing the width function by the rainfall width function (Emmanuel et al., 2015; Woods and Sivapalan, 1999). The E-GIUH is identified from data combining time series of rain fields and observed hydrographs. This E-GIUH identification has been tested on a dataset composed of 12 flood events that occurred on catchments within the OHMCV Observatory territory. Despite being of limited range, this evaluation has provided interesting insights, namely:

- The concept of E-GIUH appears to be relevant, and moreover the proposed identification method seems easily applicable and flexible for users, who are now able to define the adapted application conditions;

- The E-GIUHs associated with the various flood events of a catchment display very distinct characteristics, thus confirming that E-GIUH shape depends on the GIUH model parameters, as well as on the rainfall width function, both of which are specific to the flood events;

- For both basins, the two E-GIUH parameters (U_E, D_E) lie within the range [0.9 m/s, 1.8 m/s] for U_E and [600 m^2/s, 5,200 m^2/s] for D_E. These two parameters appear to be correlated with the event peak flow, which serves as an indicator of flow magnitude, even though this tenuous link needs to be confirmed and warrants further investigation. The identification procedure is more sensitive to parameter U_E than to parameter D_E, mainly because the direct model is not highly sensitive to this latter parameter.

- The results obtained appear to be fairly robust and in most cases remain relatively independent of the *a priori* rainfall hyetograph. This result indicates that representative E-GIUHs could be derived by defining the *a priori* effective rainfall from a widely used production function and then calibrating the two E-GIUH parameters.

This work would need to be pursued in several directions, in order to improve our knowledge and develop applications relying on the E-GIUH concept, including:

- A more robust assessment of the proposed method seems to be a priority. This could be achieved by application to a large numbers of catchments located in various climatic zones;

- The E-GIUH, which is mostly based on observed data, could be considered as a signature characterizing flood events;

- The flood events that affect a basin stem from diverse conditions: moisture status of the basin, spatial and temporal characteristics of the rain event. The E-GIUH associated with a given basin summarizes the basin response under such conditions. An analysis of the population of E-GIUHs would pave the way to a hydro-climatological catchment response to rainfall forcing;

- The relatively small number of basins and flood events described here does not allow a complete assessment of the limitations of the method under all circumstances. For instance, the method might be less suitable if the rainfall influence results from moving rainfall fields interacting with the basin (Volpi et al., 2013). In addition, the method might be less efficient when the statistical framework is outside of its application domain, e.g. when the distribution of error is not Gaussian or at least unimodal, or when the a priori conditions are not relevant.

- The E-GIUH represents a signature of the basin response that could prove useful for various applications. First, it can be used to diagnose basin responses to rainfall forcing. The E-GIUH summarizes the basin response

that stems from diverse physiographic, climatological, and meteorological conditions, such as moisture status of the basin and the spatial and temporal distribution of rainfall forcing. The E-GIUH signature can be used to compare and classify basin responses for different forcing rain events, or to analyse the influence of land use and change (e.g. recovery after wildfire) among other factors. Analysing populations of E-GIUHs that represent various conditions opens the way to hydro-climatological studies of catchment responses. Finally, it could contribute to improving lumped rainfall-runoff modelling through transfer function adapted to rainfall patterns.

Nomenclature

A	Surface area
D	Coefficient of dispersion -
E	Flood Event
$f(L, t)$	Probability density function of travel time to the catchment outlet
f_E	Event specific – GIUH
GIUH	Geomorphological Instantaneous Unit Hydrograph
E-GIUH	Event specific GIUH
L	Distance to catchment outlet along hydrological paths
$Lmax$	Maximum hydrological distance of the basin
NSE	Nash-Suttcliff efficiency criterion
pdf	Probability Density Function
$Q(t)$	Hydrograph at the outlet
$R(t)$	Hyetograph
$R_n(t)$	Effective rainfall, part of rainfall contributing to runoff
$\overline{R_e}(t)$	Areal Mean value of the effective rainfall
t	Time
U	Velocity
w	Width function at a distance
w_E	Event rainfall width function

Acknowledgments

The authors would like to express their gratitude to O.Payrastre for providing the maps of CN values for the Cevennes Region. Pierre Kirstetter acknowledges support through the NASA Ground Validation Program award NNX16AL23G.

583 **References**

584 Adamovic, M., Braud, I., Branger, F., Kirchner, J.W., 2015. Assessing the simple dynamical systems approach
585 in a Mediterranean context: Application to the Ardèche catchment (France). Hydrology and Earth
586 System Sciences 19, 2427–2449. https://doi.org/10.5194/hess-19-2427-2015
587 Alfieri, L., Smith, P.J., Thielen-Del Pozo, P.J., Beven, K.J., 2011. A staggered approach to flash flood
588 forecasting - Case study in the Cévennes region. Advances in Geosciences 29, 13–20.
589 https://doi.org/10.5194/adgeo-29-13-2011
590 Boudevillain, B., Delrieu, G., Galabertier, B., Bonnifait, L., Bouilloud, L., Kirstetter, P.E., Mosini, M.L., 2011.
591 The Cévennes-Vivarais Mediterranean Hydrometeorological Observatory database. Water Resources
592 Research 47, 1–6. https://doi.org/10.1029/2010WR010353
593 Boudhraâ, H., Cudennec, C., Andrieu, H., Slimani, M., 2018. Net rainfall estimation by the inversion of a
594 geomorphology-based transfer function and discharge deconvolution. Hydrological Sciences Journal.
595 https://doi.org/10.1080/02626667.2018.1425801
596 Chen, Y., Shi, P., Ji, X., Qu, S., Zhao, L., Dong, F., 2019. New method to calculate the dynamic factor–flow
597 velocity in Geomorphologic instantaneous unit hydrograph. Scientific Reports 9, 1–13.
598 https://doi.org/10.1038/s41598-019-50723-x
599 Choi, Y.-J., Lee, G., Kim, J.-C., 2011. Estimation of the Nash Model Parameters Based on the Concept of
600 Geomorphologic Dispersion. Journal of Hydrologic Engineering 16, 806–817.
601 https://doi.org/10.1061/(ASCE)HE.1943-5584.0000371
602 Delrieu, G., Ducrocq, V., Gaume, E., Nicol, J., Payrastre, O., Yates, E., Kirstetter, P.-E., Andrieu, H., Ayral, P.-
603 A., Bouvier, C., Creutin, J.-D., Livet, M., Anquetin, S., Lang, M., Neppel, L., Obled, C., Parent-Du-
604 Châtelet, J., Saulnier, G.-M., Walpersdorf, A., Wobrock, W., 2005. The catastrophic flash-flood event
605 of 8-9 September 2002 in the Gard Region, France: A first case study for the Cévennes-Vivarais
606 Mediterranean Hydrometeorological Observatory. Journal of Hydrometeorology 6.
607 https://doi.org/10.1175/JHM-400.1
608 Delrieu, G., Wijbrans, A., Boudevillain, B., Faure, D., Bonnifait, L., Kirstetter, P.E., 2014. Geostatistical radar-
609 raingauge merging: A novel method for the quantification of rain estimation accuracy. Advances in
610 Water Resources 71, 110–124. https://doi.org/10.1016/j.advwatres.2014.06.005
611 D'Odorico, P., Rigon, R., 2003. Hillslope and channel contributions to the hydrologic response. Water
612 Resources Research 39, 1–9. https://doi.org/10.1029/2002WR001708
613 Dolcine, L., Andrieu, H., Sempere-Torres, D., Creutin, D., 2001. Flash food forecasting with coupled
614 precipitation model in mountainous Mediterranean Basin. Journal of Hydrologic Engineering 6.
615 https://doi.org/10.1061/(ASCE)1084-0699(2001)6:1(1)
616 Dooge, J.C.I., 1959. A General Theory of the Unit Hydrograph. Journal of Geophysical Research 64, 241–256.
617 Douinot, A., Roux, H., Garambois, P.A., Dartus, D., 2018. Using a multi-hypothesis framework to improve the
618 understanding of flow dynamics during flash floods. Hydrology and Earth System Sciences 22, 5317–
619 5340. https://doi.org/10.5194/hess-22-5317-2018
620 Duband, D., Obled, C., Rodriguez, J.Y., 1993. Unit hydrograph revisited: an alternate iterative approach to UH
621 and effective precipitation identification. Journal of Hydrology 150, 115–149.
622 https://doi.org/10.1016/0022-1694(93)90158-6

623 Emmanuel, I., Andrieu, H., Leblois, E., Janey, N., Payrastre, O., 2015. Influence of rainfall spatial variability on
624 rainfall – runoff modelling : Benefit of a simulation approach ? Journal of Hydrology 531, 337–348.
625 https://doi.org/10.1016/j.jhydrol.2015.04.058
626 Emmanuel, I., Payrastre, O., Andrieu, H., Zuber, F., 2017. A method for assessing the influence of rainfall
627 spatial variability on hydrograph modeling. First case study in the Cevennes Region, southern France.
628 Journal of Hydrology 555. https://doi.org/10.1016/j.jhydrol.2017.10.011
629 Fatichi, S., Vivoni, E.R., Ogden, F.L., Ivanov, V.Y., Mirus, B., Gochis, D., Downer, C.W., Camporese, M.,
630 Davison, J.H., Ebel, B., Jones, N., Kim, J., Mascaro, G., Niswonger, R., Restrepo, P., Rigon, R., Shen,
631 C., Sulis, M., Tarboton, D., 2016. An overview of current applications, challenges, and future trends in
632 distributed process-based models in hydrology. Journal of Hydrology 537, 45–60.
633 https://doi.org/10.1016/j.jhydrol.2016.03.026
634 Fisher, C.K., Pan, M., Wood, E.F., 2020. Spatiotemporal assimilation-interpolation of discharge records through
635 inverse streamflow routing. Hydrology and Earth System Sciences 24, 293–305.
636 https://doi.org/10.5194/hess-24-293-2020
637 Goni, M., López, J.J., Gimena, F.N., 2019. Geomorphological instantaneous unit hydrograph model with
638 distributed rainfall. Catena 172, 40–53. https://doi.org/10.1016/j.catena.2018.08.010
639 Gupta, V.K., Waymire, E., Wang, C.T., 1980. A representation of an instantaneous unit hydrograph from
640 geomorphology. Water Resources Research 16, 855–862. https://doi.org/10.1029/WR016i005p00855
641 Hayami, S., 1951. On the propagation of Flood Waves. Disaster Prevention Research Institute Bulletin 1, 1–16.
642 Kirkby, M.J., 1976. Tests of the random network model, and its application to basin hydrology. Earth Surface
643 Processes 1, 197–212. https://doi.org/10.1002/esp.3290010302
644 Marani, A., Rigon, R., Rinaldo, A., 1991. A Note on Fractal Channel Networks. Water Resources Research 27,
645 3041–3049. https://doi.org/10.1029/91WR02077
646 McMillan, H., 2020. Linking hydrologic signatures to hydrologic processes: A review. Hydrological Processes
647 34, 1393–1409. https://doi.org/10.1002/hyp.13632
648 Menke, W., 2012. Geophysical Data Analysis: Discrete Inverse Theory MATLAB edition, Book.
649 https://doi.org/10.1016/B978-0-12-397160-9.00001-1
650 Moussa, R., 1997. Geomorphological transfer function calculated from digital elevation models for distributed
651 hydrological modelling. Hydrological Processes 11, 429–449. https://doi.org/10.1002/(SICI)1099-
652 1085(199704)11:5<429::AID-HYP471>3.0.CO;2-J
653 Moussa, R., Chahinian, N., Bocquillon, C., 2007. Distributed hydrological modelling of a Mediterranean
654 mountainous catchment – Model construction and multi-site validation. Journal of Hydrology 337, 35–
655 51. https://doi.org/10.1016/j.jhydrol.2007.01.028
656 Naulin, J.-P., Payrastre, O., Gaume, E., 2013. Spatially distributed flood forecasting in flash flood prone areas:
657 Application to road network supervision in Southern France. Journal of Hydrology 486, 88–99.
658 https://doi.org/10.1016/j.jhydrol.2013.01.044
659 Olivera, F., Maidment, D., 1999. Model for Runoff Routing. Water Resources Research 35, 1155–1164.
660 https://doi.org/10.1029/1998WR900104
661 Pan, M., Wood, E.F., 2013. Inverse streamflow routing. Hydrology and Earth System Sciences 17, 4577–4588.
662 https://doi.org/10.5194/hess-17-4577-2013

Rigon, R., Bancheri, M., Formetta, G., DeLavenne, A., 2016. The geomorphological unit hydrograph from a historical-critical perspective. Earth Surface Processes and Landforms 41, 27–37. https://doi.org/10.1002/esp.3855

Rinaldo, A., Marani, A., Rigon, R., 1991. Geomorphological Dispersion. Water Resources Research 27, 513–525.

Rodriguez, F., Cudennec, C., Andrieu, H., 2005. Application of morphological approaches to determine unit hydrographs of urban catchments. Hydrological Processes 19. https://doi.org/10.1002/hyp.5643

Rodriguez-Iturbe, I., Rinaldo, A., 1997. Fractal River Basins: Chance and Self-Organization, Cambridge University Press. ed.

Rodriguez-Iturbe, I., Valdés, J.B., 1979. The geomorphologic structure of hydrologic response. Water Resources Research 15, 1409–1420. https://doi.org/10.1029/WR015i006p01409

Ross, C.W., Prihodko, L., Anchang, J., Kumar, S., Ji, W., Hanan, N.P., 2018. Global Hydrologic Soil Groups (HYSOGs250m) for Curve Number-Based Runoff Modeling. https://doi.org/10.3334/ORNLDAAC/1566

Saco, P.M., Kumar, P., 2002a. Kinematic dispersion in stream networks 1. Coupling hydraulic and network geometry. Water Resources Research 38, 26-1-26–14. https://doi.org/10.1029/2001wr000695

Saco, P.M., Kumar, P., 2002b. Kinematic dispersion in stream networks 2. Scale issues and self-similar network organization. Water Resources Research 38, 27-1-27–15. https://doi.org/10.1029/2001wr000694

Saulnier, G.-M., Le Lay, M., 2009. Sensitivity of flash-flood simulations on the volume, the intensity, and the localization of rainfall in the Cévennes-Vivarais region (France). Water Resources Research 45. https://doi.org/10.1029/2008WR006906

Sherman, L.K., 1932. Stream flow from rainfall by the unit hydrograph method. Engineering News Record 501–505.

Singh, P.K., Mishra, S.K., Jain, M.K., 2014. A review of the synthetic unit hydrograph: from the empirical UH to advanced geomorphological methods. Hydrological Sciences Journal 59, 239–261. https://doi.org/10.1080/02626667.2013.870664

Smith, J.A., Baeck, M.L., Meierdiercks, K.L., Nelson, P.A., Miller, A.J., Holland, E.J., 2005. Field studies of the storm event hydrologic response in an urbanizing watershed. Water Resources Research 41. https://doi.org/10.1029/2004WR003712

Smith, J.A., Baeck, M.L., Morrison, J.E., Sturdevant-Rees, P., Turner-Gillespie, D.F., Bates, P.D., 2002. The Regional Hydrology of Extreme Floods in an Urbanizing Drainage Basin. Journal of Hydrometeorology 3, 267–282. https://doi.org/10.1175/1525-7541(2002)003<0267:TRHOEF>2.0.CO;2

Tarboton, D.G., 1997. A new method for the determination of flow directions and upslope areas in grid digital elevation models. Water Resources Research 33, 309–319. https://doi.org/10.1029/96WR03137

Tarentola, A., 2005. Inverse Problem Theory, SIAM, Society for Industrial and Applied Mathematics. ed. Philadelphie.

Tramblay, Y., Bouvier, C., Ayral, P.A., Marchandise, A., 2011. Impact of rainfall spatial distribution on rainfall-runoff modelling efficiency and initial soil moisture conditions estimation. Natural Hazards and Earth System Science 11, 157–170. https://doi.org/10.5194/nhess-11-157-2011

Vannier, O., Anquetin, S., Braud, I., 2016. Investigating the role of geology in the hydrological response of Mediterranean catchments prone to flash-floods: Regional modelling study and process understanding. Journal of Hydrology 541, 158–172. https://doi.org/10.1016/j.jhydrol.2016.04.001

Volpi, E., Di Lazzaro, M., Fiori, A., 2012. A simplified framework for assessing the impact of rainfall spatial variability on the hydrologic response. Advances in Water Resources 46, 1–10. https://doi.org/10.1016/j.advwatres.2012.04.011

Wood, E.F., Sivapalan, M., Beven, K., 1990. Similarity and scale in catchment storm response. Reviews of Geophysics 28, 1–18. https://doi.org/10.1029/RG028i001p00001

Woods, R., Sivapalan, M., 1999. A synthesis of space-time variability in storm response: Rainfall, runoff generation, and routing. Water Resources Research 35, 2469–2485. https://doi.org/10.1029/1999WR900014

Yao, C., Zhang, K., Yu, Z., Li, Z., Li, Q., 2014. Improving the flood prediction capability of the Xinanjiang model in ungauged nested catchments by coupling it with the geomorphologic instantaneous unit hydrograph. Journal of Hydrology 517, 1035–1048. https://doi.org/10.1016/j.jhydrol.2014.06.037

Zeng, Z., Tang, G., Hong, Y., Zeng, C., Yang, Y., 2017. Development of an NRCS curve number global dataset using the latest geospatial remote sensing data for worldwide hydrologic applications. null 8, 528–536. https://doi.org/10.1080/2150704X.2017.1297544

Zoccatelli, D., Borga, M., Zanon, F., Antonescu, B., Stancalie, G., 2010. Which rainfall spatial information for flash flood response modelling? A numerical investigation based on data from the Carpathian range, Romania. Journal of Hydrology 394, 148–161. https://doi.org/10.1016/j.jhydrol.2010.07.019

Appendix – Sensitivity study

This sensitivity analysis has focused on the influence of the application conditions on the identified E-GIUHs. More specifically, it has concerned: the confidence assigned to flow data (coefficient of variation α_Q), the confidence assigned to the GIUH theoretical model (coefficients of variation α_E and α_V), the influence of the *a priori* value of D_{E0}, the influence of the *a priori* value of U_{E0}, and lastly the influence of this error on the *a priori* net hyetograph.

This study has been performed by running the E-GIUH identification method while varying one of these factors with respect to the reference conditions. The influence was then assessed by calculating: i) the mean Nash efficiency criterion between the observed and resulting hydrographs (NSE_Q), ii) the mean Nash efficiency criterion between the resulting E-GIUHs and the reference E-GIUH (NSE_{GIUH}), and iii) the mean absolute deviation between the series of reference values of U_E and D_E, respectively. The results of this sensitivity analysis are displayed in Figure 8 and lead to the following conclusions:

- *Confidence assigned to flow data (*Fig. A1-a): The increase in the coefficient of variation α_Q, which reflects a loss of confidence in the measured flow data, clearly yields a reduced quality of the resulting hydrographs (blue line). The value of NSE_{GIUH} remains above 0.94, which denotes a moderate influence on the identified E- GIUH

with respect to the reference one, except for $\alpha_Q = 0.3$, where the E-GIUH change is more pronounced ($NSE_{GIUH} = 0.89$).

- *Confidence assigned to the GIUH model* (Fig. A1-b): A very strong confidence in GIUH theory ($\alpha_E = \alpha_V = 0.02$) results in a lower quality of the obtained hydrographs. This quality improves and stabilizes quickly at $NSE_Q \approx$ 0.85-0.86 as α_E and α_V increase. The value of NSE_{GIUH} is higher than 0.95 when $\alpha_E \; and \; \alpha_E \geq 0.05$, which denotes a weak influence on the identified E- GIUH with respect to the reference one. The more noteworthy effect pertains to the mean identified value of D_E, which rises from $1560\ m^2s^{-1}$ to $3700\ m^2s^{-1}$, at which point the constraints on GIUH theory are relaxed without the quality criteria being significantly modified. This finding confirms that the identification of D_E is far from being straightforward based on the available observations.

- *Influence of the a priori value of* D_{E0} (Fig. A1-c): The *a priori* value of D_{E0} has been increased from 0.35 D_{G0} to D_{G0}. The influence of this value appears to be very weak, while the values of NSE_Q and NSE_{GIUH} remain nearly constant at respectively 0.83-0.84 and 0.99. The mean identified value of D_E increases from $2110\ m^2s^{-1}$ to $2800\ m^2s^{-1}$ with respect to D_{E0}; this influence is less marked than that for α_E and α_V.

- *Influence of the a priori value of* U_{E0} (Fig. A1-d): This influence is tested by defining the *a priori* value $U_{E0} = U_E^* + \Delta U$, with U_E^* being the solution obtained according to the reference application conditions, and $\Delta U = [-0.5, 0.25, 0.0, 0.25, 0.5]\ (m/s)$. Note that a modification of U_{E0} also de facto affects D_{E0}. The results obtained indicate that: i) a strong underestimation of U_E^* ($\Delta U = -0.5\ m/s$) cannot be corrected by the identification procedure ($NSE_Q = 0.66, NSE_{GIUH} = 0.7\ and\ MAD_U = 0.2\ m/s$); ii) the situation is more satisfactory for a moderate underestimation or overestimation ($\Delta U = \pm 0.25\ m/s$), for which the final GIUHs do not differ substantially from the reference solutions ($NSE_{GIUH} = 0.92\ and\ 0.93$ and $MAD_U = 0.11\ and\ 0.09 m/s$, respectively), and iii) an initial overestimation of velocity by the *a priori* value appears to be less detrimental than an underestimation.

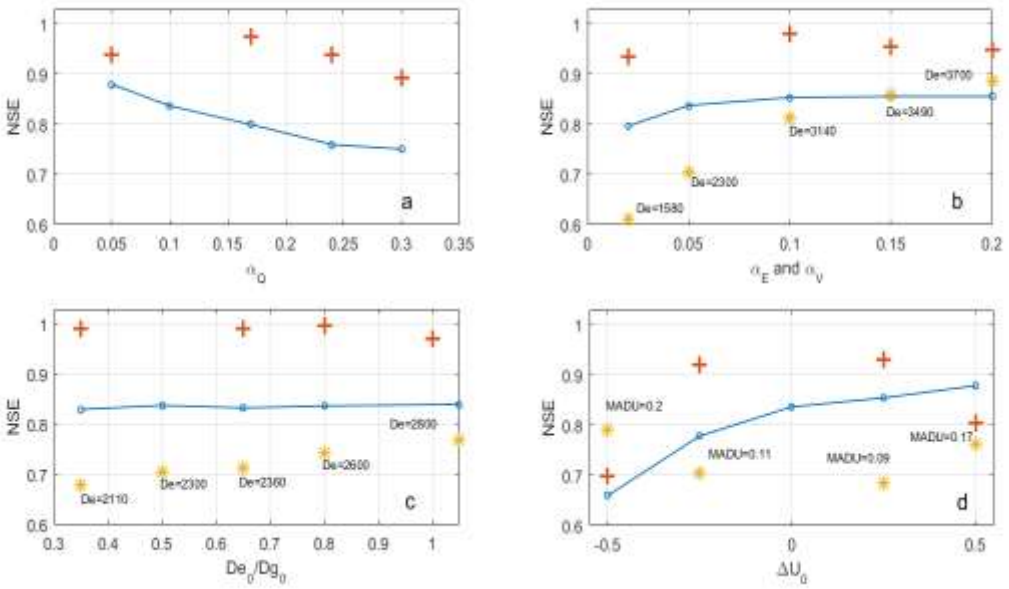

Figure A1: Sensitivity study of the E-GIUH identification: (A) influence of α_Q, (B) : influence of α_E and α_V, (C) : influence of the *a priori* value D_{E0}; (D) : Influence of the *a priori* celerity U_{E0} NSE_Q (blue line), NSE_{GIUH} (red crosses),

- *Influence of this error covariance on the a priori net hyetograph.*

The E-GIUH identification has been performed by varying the value of α_R from α_R =0.03 (excellent confidence in the *a priori* net hyetograph) to $\alpha_R = 0.30$ (weak confidence). These results are illustrated in Figure A2, in its display of the evolution in NSE_Q between the observed hydrographs and the hydrographs simulated using the final set of parameters, in offering the following insights:

- The increase of α_R results in an increase of NSE_Q, which rises from $NSE_Q = 0.83$ for $\alpha_R = 0.03$ to $NSE_Q = 0.88$ for $\alpha_R = 0.24$, meaning that the set of parameters characterizing basin operations ($\overline{\boldsymbol{R_n}}$, $\boldsymbol{EGIUH}$) is globally better determined.

- This improvement is not correlated with significant changes in the identified E-GIUHs, which do not differ significantly from the E-GIUH reference application conditions. Indeed, the value of NSE_{GIUH} remains above 0.97 for $\alpha_R = 0.17$ and $\alpha_R = 0.24$.

- This improvement is mainly derived from changes in the resulting net hyetographs, in comparison with the *a priori* net hyetographs, as confirmed by the value of NSE_{Rn} calculated between the *a priori* and identified net hyetographs, which decreases from 0.99 to 0.55 as α_R increases from 0.05 to 0.3.

This sensitivity analysis has confirmed that relaxing the constraint on the *a priori* net hyetograph yields an overall more efficient functioning of the identification algorithm, which leads to a coupled identification of the

781 ($\overline{\boldsymbol{R_n}}, \boldsymbol{EGIUH}$) couple without modifying the resulting E-GIUH by considering the *a priori* net hyetograph to be

782 accurate.

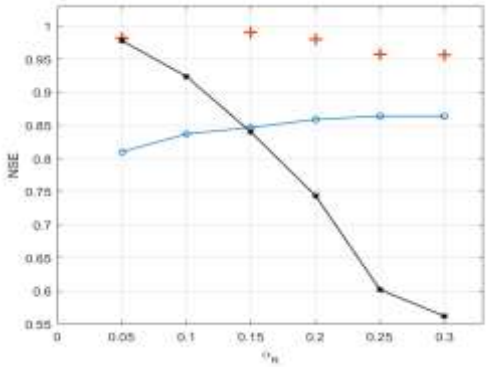

783

784 Figure A2 : Sensitivity study of the E-GIUH identification to the application conditions : influence of α_R

785 NSE_Q (blue line), NSE_{GIUH} (red crosses), NSE_{Rn} (black line)